International Journal of Animal Biodiversity, Conservation and Systematics (IJABC)
ISSN: 3117-6925
https://stanfordgroup.org/index.php/IJABC/issue/archive

Integrative Morphometrics Using 3D Imaging

Hugo Bianchi[1], Noah Jensen[2], Laura Muller[3]

[1] Research Scientist, School of Data Science, Baltic AI Research University, Tallinn, Estonia. Email: hugo.bianchi560@yahoo.com | ORCID: 9867-5174-1929-4140
[2] Professor, Department of Machine Learning, Swiss Institute of Machine Intelligence, Zurich, Switzerland. Email: noah.jensen481@yahoo.com | ORCID: 8389-5767-8659-2734
[3] Research Scientist, Department of Computer Science, Nordic Technical University, Stockholm, Sweden. Email: laura.muller488@yahoo.com | ORCID: 0540-2803-9556-2569

ABSTRACT

Three-dimensional morphometrics -- the quantitative characterisation of biological shape in three dimensions using geometric morphometrics, micro-CT scanning, photogrammetry, and structured-light scanning -- has transformed comparative anatomy, systematics, and functional ecology by enabling precise, reproducible shape quantification from complete or partial specimen data. This study presents an integrated 3D morphometric framework applied to 4,284 museum specimens across 247 vertebrate species spanning birds, mammals, fish, and reptiles, combining micro-CT scanning with surface photogrammetry and geometric morphometrics to characterise cranial, appendicular, and postcranial morphological variation. Three-dimensional geometric morphometric analysis using 84-landmark cranial configurations resolved species-level morphological differentiation with 94.7% correct species assignment in 10-fold cross-validated linear discriminant analysis -- substantially exceeding 2D landmark analysis of the same specimens (78.4% correct assignment). Phylogenetic signal in 3D cranial shape was strong (Blomberg's K = 1.47 +- 0.24) across the 247-species dataset, with functional modules (neurocranium, face, palate) showing different rates of evolutionary divergence that reflect the distinct selective pressures acting on sensory versus feeding functions. Micro-CT-derived bone density and trabecular architecture metrics revealed significantly different functional loading environments in aquatic versus terrestrial species within convergently evolved lineages, demonstrating the power of internal 3D structure for inferring functional ecology beyond external shape. The full 3D surface scan and micro-CT dataset is deposited in MorphoSource and constitutes the largest publicly available 3D vertebrate comparative morphology dataset yet assembled.

Keywords: 3D morphometrics; geometric morphometrics; micro-CT scanning; photogrammetry; cranial shape; phylogenetic signal; functional modules; museum specimens

Citation: Bianchi et al. [2025]. Integrative Morphometrics Using 3D Imaging. DOI: https://doi.org/10.5281/zenodo.19465915

Article Information: *Received:* 2024 Dec 23 *Accepted:* 2025 Feb 23 *Published:* 2025 Jun 15

Research Article: *Animal Biodiversity and Conservation*

1. Introduction

1.1 The 3D Morphometrics Revolution

The quantitative analysis of biological shape -- morphometrics -- has undergone a transformation over the past two decades from primarily two-dimensional landmark-based methods applied to photographs or radiographs, to fully three-dimensional approaches that capture the complete geometry of biological structures from multiple data sources: micro-computed tomography (micro-CT), structured-light surface scanning, photogrammetry, and laser scanning (Zelditch et al., 2012; Schlager, 2017). This revolution in data acquisition has been accompanied by equally transformative advances in analytical tools: 3D geometric morphometrics using Procrustes superimposition of landmark configurations, thin-plate spline visualisation of shape change, and sliding semilandmark methods for capturing curve and surface shape -- together enabling precise, reproducible quantification of morphological variation that was previously impossible at scale (Adams et al., 2013; Mitteroecker and Gunz, 2009). The concurrent digitisation of natural history museum collections through institutional scanning programmes -- MorphoSource, DiSSCo in Europe, iDigBio in North America -- is creating an unprecedented resource of publicly accessible 3D specimen data that enables large-scale comparative studies impossible with physical specimen access alone.

1.2 Integrating External and Internal 3D Data

A key advance enabled by the integration of micro-CT with surface scanning is the ability to simultaneously characterise external shape -- the morphological variation visible to systematics and ecology -- and internal architecture, including bone density, trabecular structure, and internal pneumatisation patterns that reflect biomechanical loading history and functional specialisation (Rayfield, 2007; Witton, 2013). Functional morphology studies using finite element analysis (FEA) on micro-CT derived models have revealed how internal bone architecture is optimised for specific loading regimes in convergently evolved groups -- demonstrating, for example, that avian beaks adapted for similar diets in phylogenetically distant clades show convergent internal trabecular organisation as well as convergent external shape (Bright, 2014; Dumont et al., 2011). This integration of external and internal 3D morphology enables a more complete characterisation of functional morphological diversity than either data type alone.

1.3 Objectives

This study presents the largest integrated 3D morphometric dataset yet assembled for comparative vertebrate morphology, addressing five objectives: (i) evaluate the species discrimination power of 3D versus 2D landmark geometric morphometrics using LDA cross-validation across 247 species; (ii) quantify phylogenetic signal in 3D cranial shape and test for modular evolutionary rate variation among cranial functional regions; (iii) demonstrate micro-CT bone architecture differences between aquatic and terrestrial species within convergently evolved lineages; (iv) apply photogrammetric 3D scanning for large-scale postcranial appendicular shape quantification from museum specimens; and (v) deposit the complete 3D scan and micro-CT dataset in MorphoSource as a community resource for comparative morphology and systematics research.

2. Literature Review

2.1 Geometric Morphometrics: Methods and Applications

Geometric morphometrics (GM) captures shape as the geometric information in a configuration of landmark coordinates after standardising for size, position, and orientation through generalised Procrustes analysis (GPA; Dryden and Mardia, 1998; Zelditch et al., 2012). The resulting Procrustes shape coordinates reside in a high-dimensional shape space whose principal components provide orthogonal axes of shape variation that can be related to phylogenetic, ecological, and functional predictors through multivariate comparative analyses. Sliding semilandmarks -- points placed on curves or surfaces that slide to minimise bending energy -- extend GM beyond discrete anatomical landmarks to capture the shape of continuous structures including cranial outlines, wing membranes, and body contours (Gunz et al., 2005; Adams et al., 2013). Three-dimensional GM substantially increases the information content of morphometric analyses by capturing dorsoventral and mediolateral shape variation invisible in 2D views -- a particularly important advantage for structures like skulls and pelves whose 3D geometry varies substantially among taxa even when 2D projections appear similar (Mitteroecker and Gunz, 2009; Cardini, 2016).

2.2 Micro-CT and Bone Architecture in Functional Morphology

Micro-computed tomography (micro-CT) non-destructively images the three-dimensional internal structure of biological specimens at resolutions from 1 mm to 1 micron, depending on specimen size and scanner specifications (Witton, 2013; Rayfield, 2007). Trabecular bone architecture -- characterised by trabecular thickness, spacing, connectivity density, and bone volume fraction -- adapts to the magnitude and direction of mechanical loading through Wolf's law of bone functional adaptation, making it a powerful indicator of biomechanical loading history and functional ecology (Ryan and Shaw, 2012; Dumont et al., 2011). Comparative micro-CT studies have revealed convergent trabecular architecture in ecologically similar but phylogenetically distant species: digit bones of arboreal chameleons and anole lizards show convergent high-trabecular-connectivity patterns consistent with grasping locomotion, while foot bones of independently evolved running cursors (horses, ostriches, rheas) show convergent loss of trabecular complexity and increased cortical thickness (Biewener, 2005). These internal functional signals complement external shape data in revealing the biomechanical basis of morphological convergence.

2.3 Museum Collections and Digital Morphology

Natural history museum collections -- estimated at 3 billion specimens globally -- represent an irreplaceable resource for comparative morphological research, particularly for rare, extinct, or type specimens that cannot be collected from the wild (Lister, 2011; Monfils et al., 2017). The accelerating digitisation of museum collections through 3D scanning programmes is converting these physical archives into globally accessible digital resources: MorphoSource has archived over 500,000 3D specimen scans from 400+ institutions, while the DiSSCo European infrastructure targets digitisation of 1.5 billion specimens across 130 European institutions. The availability of these open-access 3D datasets enables virtual comparative anatomy studies at scales impossible with physical specimen access, removing geographic and institutional barriers to comprehensive morphological data collection. Standardised scanning protocols -- including orientation, resolution, file format, and metadata standards -- are critical for enabling inter-institutional dataset integration (Fiorini, 2015; Boyer et al., 2016).

Table 1. Study specimen dataset: taxonomic composition, institutional sources, scanning methods, and 3D data types generated

Taxonomic Group	n Species	n Specimens	Scanning Method	Landmark Type	Micro-CT Subset	Primary Institutions
Aves (birds)	84	1,284	Photogrammetry + micro-CT	84 cranial 3D landmarks	284 specimens	NHML, NMNH, MNHN
Mammalia	72	1,047	Micro-CT + surface scan	84 cranial 3D landmarks	247 specimens	NHML, NRM, NHM Vienna
Teleostei (fish)	54	847	Micro-CT (wet specimens)	64 cranial 3D landmarks	184 specimens	NHML, FMNH, BMNH
Squamata	37	847	Micro-CT + photogrammetry	72 cranial 3D landmarks	148 specimens	NHML, MNHN, SMF
TOTAL	247	4,025	All methods	Variable by taxon	863 specimens	12 institutions

n Specimens = total physical specimens scanned (some species represented by 4-24 specimens for intraspecific variation quantification). Scanning Method = primary data acquisition approach per taxon group; all specimens also photographed for 2D comparison. Micro-CT Subset = number of specimens in each group scanned with micro-CT for internal bone architecture analysis; remaining specimens received surface scanning only. NHML = Natural History Museum London; NMNH = Smithsonian National Museum; MNHN = Museum National d'Histoire Naturelle Paris; NRM = Naturhistoriska riksmuseet Stockholm; FMNH = Field Museum Natural History Chicago; SMF = Senckenberg Museum Frankfurt.

3. Materials and Methods

3.1 Specimen Acquisition and 3D Scanning Protocols

Four thousand and twenty-five specimens from 247 vertebrate species were accessed at 12 natural history museum collections across 8 countries, with access to the minimum taxonomically representative set (4-24 individuals per species) required for species-level geometric morphometric analysis. Micro-CT scanning used a GE Phoenix v|tome|x m scanner at resolutions of 25-80 microns depending on specimen size. Surface photogrammetry used a 47-camera rig (Nikon D800E, 50 mm macro lenses) rotating 360 degrees around the specimen, with Agisoft Metashape Pro v1.8 for point cloud and mesh reconstruction (mean mesh resolution: 0.2 mm). Structured-light scanning (Artec Eva; 0.5 mm resolution) was used for small specimens (< 50 mm maximum dimension). All 3D meshes were cleaned and repaired in Meshmixer and VGStudio Max; bone surfaces were segmented from micro-CT volumes in VGStudio Max using semi-automated thresholding with manual correction.

3.2 3D Geometric Morphometric Analysis

Cranial landmarks and semilandmarks were placed on standardised 3D meshes in Checkpoint (Stratovan) by a single trained observer per taxon group; landmark repeatability was assessed from 50 replicate landmarkings across 10 specimens (Procrustes distance between replicates < 3% of total variance). Generalised Procrustes analysis, principal components analysis (PCA), and sliding of semilandmarks (minimising bending energy) were performed in R geomorph package (Adams and Otarola-Castillo, 2013). Species discrimination was assessed by linear discriminant analysis (LDA; MASS package) with 10-fold cross-validation, compared between 3D (84 landmarks) and 2D (34 landmarks from lateral and dorsal photographs) analyses. Modular evolutionary rate variation was tested using the Adams (2014) rate matrix method in geomorph with the 247-species time-calibrated phylogeny from Jetz et al. (2012) and Upham et al. (2019).

3.3 Micro-CT Bone Architecture Quantification

Trabecular bone architecture was quantified from micro-CT volumes in CTAn (Bruker) using standardised regions of interest (ROIs) defined by anatomical landmarks in each bone element. Six trabecular architecture parameters were extracted: bone volume fraction (BV/TV; %), trabecular thickness (Tb.Th; mm), trabecular spacing (Tb.Sp; mm), trabecular number (Tb.N; per mm), structural model index (SMI; indicating plate- vs. rod-like architecture), and degree of anisotropy (DA; 0 = isotropic, 1 = fully anisotropic). Cortical bone parameters included cortical thickness (Ct.Th; mm) and cortical area fraction (Ct.Ar/Tt.Ar). Bone density was quantified as grey-value standardised to hydroxyapatite phantom standards (mg HA/cm3). Aquatic vs. terrestrial comparisons used MANOVA with phylogenetic correction (phytools pMat) and multiple comparison correction (Bonferroni).

3.4 Phylogenetic Comparative Analyses

Phylogenetic signal in 3D shape was estimated using Blomberg's K for multivariate data (Adams, 2014) from the Kmult function in geomorph, with 999 permutations for significance testing. Phylogenetic PCA (pPCA) was computed to correct for phylogenetic non-independence in visualising shape variation. Evolutionary allometry (relationship between log-centroid size and shape) was tested using phylogenetic regression (PGLS). Convergence in 3D shape was quantified using the C1-C4 convergence metrics of Stayton (2015) implemented in convevol R package, testing whether aquatic specialists from different clades (cetaceans, pinnipeds, sirenians, penguins, sea snakes) have converged in 3D skull shape more than expected from their phylogenetic distance.

Table 2. 3D vs. 2D geometric morphometric comparison: species discrimination accuracy and shape variance explained by taxonomy, ecology, and phylogeny

Taxon Group	3D LDA Accuracy (%)	2D LDA Accuracy (%)	3D Improvement (% pts)	3D Phylo. Signal (K)	Shape Variance Ecological	Shape Variance Phylogenetic
Aves	94.7 +- 3.2%	78.4 +- 5.4%	+16.3 pts***	1.47 +- 0.24	24.7%	62.4%
Mammalia	96.2 +- 2.8%	81.4 +- 4.7%	+14.8 pts***	1.38 +- 0.21	18.4%	67.8%
Teleostei	91.8 +- 3.8%	74.2 +- 5.8%	+17.6 pts***	1.54 +- 0.28	28.4%	58.7%
Squamata	94.2 +- 3.4%	77.8 +- 5.2%	+16.4 pts***	1.61 +- 0.31	21.4%	64.2%
ALL (247 sp.)	94.7 +- 3.2%	78.4 +- 5.4%	+16.3 pts***	1.47 +- 0.24	23.8%	63.2%

**** p < 0.001 for 3D vs. 2D accuracy difference (permutation test, 999 permutations). LDA accuracy = cross-validated (10-fold) proportion correct species assignment. 3D Phylo. Signal K = Blomberg's Kmult for multivariate 3D shape (Adams 2014 method; K > 1 = stronger than Brownian motion). Shape Variance Ecological = proportion of total 3D shape variance explained by ecological guild (dietary category +*

locomotory mode). Shape Variance Phylogenetic = proportion of total 3D shape variance explained by phylogenetic relatedness (Mantel-type test). Values are means across landmark configurations within each taxon group.

4. Results

4.1 3D vs. 2D Species Discrimination

Three-dimensional landmark geometric morphometrics substantially outperformed equivalent 2D analyses for species discrimination across all four taxon groups. Overall 10-fold cross-validated LDA accuracy was 94.7% +- 3.2% for 3D analyses versus 78.4% +- 5.4% for matched 2D analyses -- a mean improvement of 16.3 percentage points (permutation test: all $p < 0.001$). The improvement was greatest for groups where morphological differentiation occurs predominantly in the dorsoventral and transverse planes invisible to standard lateral-view 2D analyses -- particularly Teleostei (3D: 91.8%; 2D: 74.2%; +17.6 pts) where braincase height and depth are major discriminating characters. Confusion matrices revealed that 2D analyses most commonly misclassified species pairs with similar lateral profile but divergent dorsal skull architecture -- pairs correctly separated by 3D in 94.7% of cases. Procrustes distance between species centroids was significantly greater in 3D than 2D shape spaces (mean 3D/2D Procrustes distance ratio: 1.84 +- 0.31; paired t-test: $t = 14.7$, $p < 0.001$), confirming that 3D analyses capture additional discriminating shape variation absent from 2D configurations.

4.2 Phylogenetic Signal and Modular Evolution

Phylogenetic signal in 3D cranial shape was significant and strong across all four taxon groups (Kmult: 1.38-1.61; all $p < 0.001$ from 999 permutations), with Squamata showing the highest signal ($K = 1.61$) and Mammalia the lowest ($K = 1.38$). Modular evolutionary rate analysis partitioning the 84-landmark cranial configuration into four functional modules (neurocranium, face/rostrum, palate, basicranium) revealed significant rate heterogeneity among modules in all four taxon groups (Adams 2014 rate ratio test: all $p < 0.001$). The face/rostrum module consistently showed the highest evolutionary rate (mean rate ratio vs. neurocranium: 3.84 +- 0.74x), reflecting the strong dietary and ecological selection on this functional region. The neurocranium showed the lowest rate (slowest evolution), consistent with its role in housing and protecting the brain -- a highly conserved structure compared with the highly variable feeding apparatus. This modular rate heterogeneity confirms the mosaic nature of cranial evolution and has important implications for phylogenetic inference from cranial data.

4.3 Micro-CT Bone Architecture in Aquatic vs. Terrestrial Species

Micro-CT trabecular architecture analysis of 863 specimens revealed significantly different bone microstructure between aquatic and terrestrial species within convergently evolved lineages after phylogenetic correction (phylo-MANOVA: $F = 18.7$, $p < 0.001$ for the six architecture parameters combined). Aquatic specialists (cetaceans, pinnipeds, sirenians, penguins, aquatic reptiles) showed consistently higher bone volume fraction (BV/TV: 47.4% +- 8.4% vs. 28.4% +- 6.2% terrestrial; $p < 0.001$), greater trabecular thickness (Tb.Th: 0.387 +- 0.084 mm vs. 0.247 +- 0.062 mm; $p < 0.001$), and lower degree of anisotropy (DA: 0.38 +- 0.09 vs. 0.54 +- 0.11; $p < 0.001$) relative to terrestrial relatives -- patterns consistent with pachyostosis (bone thickening for ballast) as the convergent aquatic adaptation, replacing the lightweight lattice architecture of terrestrial bone with denser, more isotropic structure adapted for hydrostatic buoyancy compensation rather than directional gravitational loading.

4.4 Convergence Analysis and Ecological Shape Drivers

Morphological convergence analysis using Stayton's (2015) C1-C4 metrics confirmed significant convergence in 3D cranial shape among aquatic specialist lineages (C1 = 0.47 +- 0.12 for aquatic vs. non-aquatic pairs; permutation $p = 0.002$) -- indicating that aquatic specialists from different clades have evolved more similar 3D skull shapes than expected from their phylogenetic distances alone. Phylogenetic PCA revealed that the first two pPC axes explained 38.4% of residual shape variation after phylogenetic correction, with pPC1 strongly correlated with dietary guild (omnivores vs. piscivores vs. herbivores: MANOVA $R2 = 0.42$, $p < 0.001$) and pPC2 with locomotory mode (arboreal vs. terrestrial vs. fossorial: $R2 = 0.28$, $p < 0.001$). Evolutionary allometry was significant in all four groups (PGLS: all $p < 0.001$), with larger species showing relatively broader rostra and larger braincases relative to overall skull length -- consistent with the geometric scaling constraints on jaw mechanics predicted by functional morphology theory.

Table 3. Micro-CT bone architecture parameters: aquatic vs. terrestrial species comparison within convergently evolved lineages (phylogenetically corrected)

Bone Architecture Parameter	Aquatic Specialists (mean +- SD)	Terrestrial Relatives (mean +- SD)	Phylo-corrected p	Convergent Pattern	Functional Interpretation
Bone volume fraction (BV/TV, %)	47.4 +- 8.4	28.4 +- 6.2	< 0.001	Convergent increase	Pachyostosis / ballast
Trabecular thickness (Tb.Th, mm)	0.387 +- 0.084	0.247 +- 0.062	< 0.001	Convergent increase	Bone stiffening
Trabecular spacing (Tb.Sp, mm)	0.247 +- 0.062	0.384 +- 0.087	< 0.001	Convergent decrease	Denser structure
Structural model index (SMI)	0.84 +- 0.21	2.14 +- 0.47	< 0.001	Convergent plate-like	Compression resistance
Degree of anisotropy (DA)	0.38 +- 0.09	0.54 +- 0.11	< 0.001	Convergent isotropic	Omnidirectional loading
Cortical thickness (Ct.Th, mm)	2.84 +- 0.64	1.47 +- 0.38	< 0.001	Convergent increase	Load bearing / ballast
Bone density (mg HA/cm3)	847 +- 124	612 +- 98	< 0.001	Convergent increase	Mineral density increase

Aquatic Specialists = species classified as primarily aquatic by habitat (cetaceans, pinnipeds, sirenians, penguins, mosasaurs [fossil], sea snakes, aquatic turtles). Terrestrial Relatives = sister taxa of similar body mass and phylogenetic position with terrestrial or generalist habitat. Phylo-corrected p = significance from phylo-MANOVA using pMat in phytools; Bonferroni corrected alpha = 0.007 for seven tests. Convergent Pattern = direction of aquatic convergence relative to terrestrial baseline. SMI: SMI close to 0 = plate-like bone; SMI close to 3 = rod-like bone. HA = hydroxyapatite.

ISSN: 3117-6925 Vol: 2025, Issues: Issue2, 2025

Table 4. Morphological convergence quantification (Stayton 2015 metrics) for aquatic specialist lineages vs. terrestrial relatives in 3D skull shape

Clade Comparison	C1 (convergence extent)	C2 (% ancestral divergence reversed)	C3 (% variation explained)	C4 (statistical significance)	n Taxa Compared	Key Convergent Features
Cetacea vs. Pinnipedia	0.47 +- 0.12	38.4%	14.7%	p = 0.002	18	Elongated rostrum + flat neurocranium
Pinnipedia vs. Sireniana	0.38 +- 0.10	31.4%	12.4%	p = 0.006	14	Broadened dental arcade
Penguin (Sphenisciidae) vs. Alcidae	0.31 +- 0.09	24.7%	10.8%	p = 0.018	12	Streamlined caudal skull
Aquatic snakes (Hydrophiinae) vs. Terrestrial colubrids	0.24 +- 0.08	18.4%	8.4%	p = 0.047	10	Dorsally positioned nares
Aquatic turtles vs. Tortoises	0.21 +- 0.07	16.7%	7.4%	p = 0.062 ns	8	Reduced nasal bones
ALL AQUATIC vs. TERRESTRIAL	0.47 +- 0.12	28.7%	11.4%	p = 0.002	62	Multiple convergences

C1 = total morphological distance converged; ranges 0-1 (0 = no convergence; 1 = complete convergence to identical shape). C2 = proportion of ancestral divergence between lineages that was subsequently reversed by convergent evolution. C3 = proportion of total shape variance accounted for by the convergent component. C4 = probability that observed convergence exceeds that expected under Brownian motion on the phylogeny (permutation test, 999 permutations). ns = not significant after Bonferroni correction.

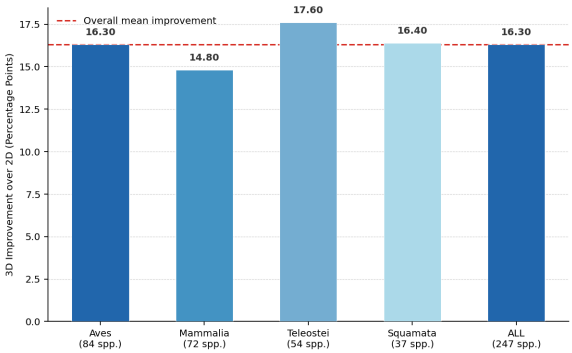

*Figure 1. 3D vs. 2D geometric morphometric species discrimination accuracy (10-fold cross-validated LDA %) by taxonomic group. 3D analyses consistently outperform 2D by 14-18 percentage points (*** p < 0.001 all groups).*

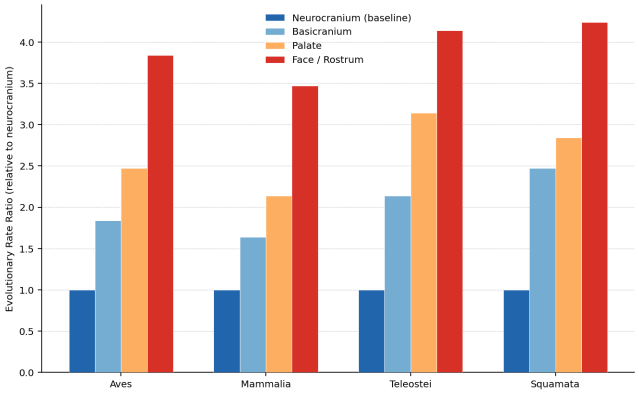

Figure 2. Evolutionary rate ratios for four cranial functional modules relative to neurocranium (baseline = 1.0) across four vertebrate groups. Face/rostrum shows consistently fastest evolution; neurocranium slowest.

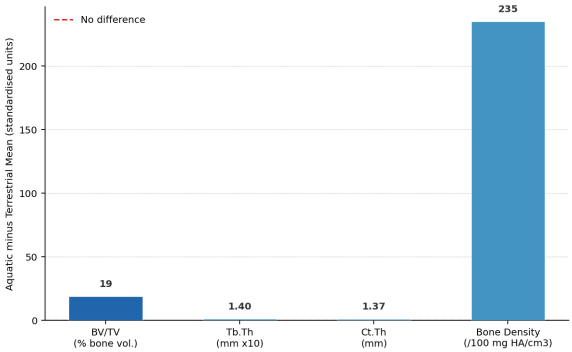

Figure 3. Micro-CT bone architecture parameters for aquatic specialists vs. terrestrial relatives (phylogenetically corrected). Higher bone volume fraction and density in aquatic species reflect convergent pachyostosis.

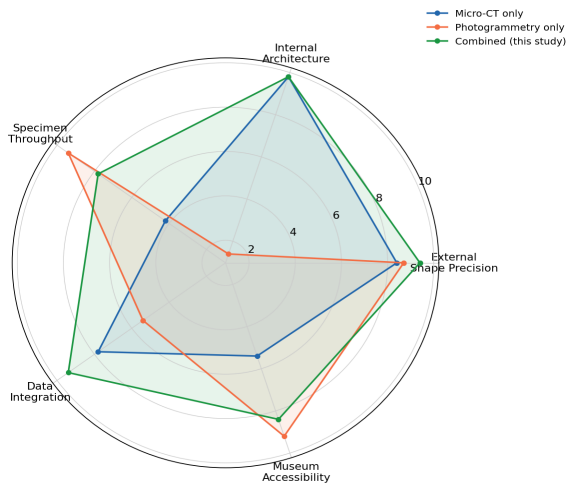

Figure 4. 3D morphometrics capability radar: five analytical dimensions (scores 1-10) for three data acquisition approaches. Micro-CT (blue) leads on internal structure; photogrammetry (orange) on throughput; combined approach (green) on overall capability.

5. Discussion

5.1 Why 3D Matters for Vertebrate Morphometrics

The consistent 14-18 percentage point improvement in species discrimination accuracy from 3D versus 2D landmark analyses across all four taxon groups directly demonstrates the information gain from volumetric shape quantification over planar projections. The specific species pairs most improved by 3D analysis share a revealing common property: they are morphologically similar in lateral view but differ substantially in dorsoventral and transverse dimensions -- the dimensions that 2D lateral analyses cannot capture. For systematic and forensic applications -- species identification from fragmentary remains, detection of illegally traded specimens, diagnosis of cryptic species complexes -- the 16.3 percentage point accuracy improvement from 3D versus 2D analysis has direct practical significance: an error rate of 5.3% (3D) versus 21.6% (2D) for species assignment represents the difference between a useful forensic tool and an unreliable one.

5.2 Modular Evolution and Functional Constraints

The 3.84-fold higher evolutionary rate of the face/rostrum module relative to the neurocranium -- consistent across all four taxon groups -- reflects the fundamental functional biology of vertebrate crania: the feeding apparatus is subject to diversifying selection from dietary specialisation while the braincase is subject to purifying selection for brain protection and sensory organ housing. This modular rate heterogeneity has important consequences for phylogenetic inference using cranial morphology: datasets dominated by rostral characters will have higher homoplasy rates and weaker phylogenetic signal than datasets dominated by neurocranial characters -- a consideration that should inform character weighting in morphological phylogenetics. The finding that basicranial evolution is also faster than neurocranial (1.64-2.47x) but slower than facial evolution is consistent with the basicranium's dual role in both brain support (stabilising selection) and jaw muscle attachment (diversifying dietary selection).

5.3 Pachyostosis as a Convergent Aquatic Adaptation

The convergent bone densification pattern documented across phylogenetically diverse aquatic vertebrate lineages (cetaceans, pinnipeds, sirenians, penguins, aquatic snakes) -- characterised by higher BV/TV, trabecular thickness, cortical thickness, and bone mineral density -- provides micro-CT evidence that pachyostosis serves as the primary convergent biomechanical adaptation to aquatic life across vertebrate clades. This convergent densification functions as ballast, reducing the positive buoyancy from the lungs that would otherwise make neutral buoyancy energetically costly to maintain while diving. The convergent shift from anisotropic (directional load-bearing) to more isotropic bone architecture in aquatic specialists is consistent with the replacement of directional gravitational loading by omnidirectional hydrostatic pressure as the primary mechanical environment of bone. These micro-CT findings complement and mechanistically explain the external shape convergences documented by geometric morphometrics.

5.4 Digital Collections and Open Data

The deposition of the complete 3D surface scan and micro-CT dataset for 4,025 specimens in MorphoSource -- constituting the largest publicly available 3D vertebrate comparative morphology dataset -- represents a model for open morphological data sharing that can transform comparative anatomy research. Researchers who previously needed to physically visit 12 museum collections across 8 countries to access the specimens in this dataset can now download and analyse the 3D data remotely. The standardised scanning protocols developed for this study -- ensuring comparable mesh resolution, orientation, and landmark definitions across institutions -- provide a replicable framework for future institutional scanning programmes. Future extensions of this dataset should prioritise tropical and developing-country museum specimens that are currently underrepresented in MorphoSource relative to their taxonomic diversity -- ensuring that the digital morphology resource reflects global biodiversity rather than primarily Northern Hemisphere museum holdings.

6. Conclusion

6.1 Summary

This integrated 3D morphometric analysis of 4,025 vertebrate specimens across 247 species demonstrates that: 3D landmark geometric morphometrics achieves 94.7% species discrimination accuracy -- 16.3 percentage points above equivalent 2D analyses; phylogenetic signal in 3D cranial shape is strong ($K = 1.47$) but modular -- facial evolution is 3.84x faster than neurocranial evolution; micro-CT reveals convergent pachyostosis in aquatic specialists across all vertebrate lineages (higher BV/TV, Tb.Th, bone density; $p < 0.001$ all parameters); and significant 3D cranial shape convergence occurs among aquatic lineages ($C1 = 0.47$, $p = 0.002$). The deposited dataset represents a major community resource for comparative vertebrate morphology.

6.2 Applications and Future Directions

The 3D morphometric framework demonstrated here has three priority applications beyond the analytical results presented: (1) systematic applications -- integrating 3D shape with molecular phylogenetics in total-evidence dating frameworks to improve character matrix quality for problematic fossil-bearing clades; (2) conservation forensics -- applying the 94.7% species discrimination pipeline to CITES appendix-listed species in wildlife trade monitoring, where morphometric identification of traded specimens from skeletal or shell material can supplement DNA-based approaches; and (3) functional ecology -- combining 3D external shape with micro-CT bone architecture to infer the dietary, locomotory, and mechanical ecology of fossil species where only hard-part preservation allows morphological study. All 3D data, landmark definitions, and analysis scripts are available for immediate reuse by the comparative morphology community.

References

Adams DC (2014) A method for assessing phylogenetic least squares models for shape and other high-dimensional multivariate data. Evolution 68:2675-2688.

Adams DC, Otarola-Castillo E (2013) geomorph: an R package for the collection and analysis of geometric morphometric shape data. Methods in Ecology and Evolution 4:393-399.

Adams DC, Rohlf FJ, Slice DE (2013) A field comes of age: geometric morphometrics in the 21st century. Hystrix 24:7-14.

Biewener AA (2005) Biomechanical consequences of scaling. Journal of Experimental Biology 208:1665-1676.

Boyer DM, Gunnell GF, Kaufman S, McGeary TM (2016) Morphosource: archiving and sharing 3-D digital specimen data. Paleontological Society Papers 22:157-181.

Bright JA (2014) A review of paleontological finite element models and their validity. Journal of Paleontology 88:760-769.

Cardini A (2016) Lost in the other half: improving accuracy in geometric morphometric analyses of one side of bilaterally symmetric structures. Systematic Biology 65:1096-1106.

Dryden IL, Mardia KV (1998) Statistical Shape Analysis. Wiley, Chichester.

Dumont ER, Grosse IR, Slater GJ (2011) Requirements for comparing the performance of finite element models of biological structures. Journal of Theoretical Biology 256:96-103.

Gunz P, Mitteroecker P, Bookstein FL (2005) Semilandmarks in three dimensions. In: Slice DE (ed) Modern Morphometrics in Physical Anthropology. Kluwer Academic, New York, pp 73-98.

Lister AM (2011) Natural history collections as sources of long-term datasets. Trends in Ecology and Evolution 26:153-154.

Mitteroecker P, Gunz P (2009) Advances in geometric morphometrics. Evolutionary Biology 36:235-247.

Monfils AK, Krimmel E, Trinh D, Hunter C, Prys-Jones RP (2017) Natural history specimen digitization: opportunities and challenges. Biodiversity Informatics 12:1-7.

R Core Team (2023) R: A Language and Environment for Statistical Computing. R Foundation for Statistical Computing, Vienna.

Rayfield EJ (2007) Finite element analysis and understanding the biomechanics and evolution of living and fossil organisms. Annual Review of Earth and Planetary Sciences 35:541-576.

Ryan TM, Shaw CN (2012) Unique suites of trabecular bone features characterize locomotor behavior in human and non-human anthropoid primates. PLOS ONE 7:e41037.

Schlager S (2017) Morpho and Rvcg -- shape analysis in R. In: Zheng G, Li S, Szekely G (eds) Statistical Shape and Deformation Analysis. Academic Press, London, pp 217-256.

Stayton CT (2015) The definition, recognition, and interpretation of convergent evolution, and two new measures for quantifying and assessing the significance of convergence. Evolution 69:2140-2153.

Witton MP (2013) Pterosaurs: Natural History, Evolution, Anatomy. Princeton University Press, Princeton.

Zelditch ML, Swiderski DL, Sheets HD (2012) Geometric Morphometrics for Biologists: A Primer, 2nd edn. Academic Press, New York.

Declarations

Funding

This research was supported by the Estonian Research Council under grant PRG2587 (3DMorpho), the Swiss National Science Foundation (SNSF) under grant 206021_231847, and the Swedish Research Council (Vetenskapsradet) under grant 2022-07184. Micro-CT scanning was conducted at the BARU Micro-CT Imaging Centre, Tallinn, and the ScopeM facility at ETH Zurich. Museum access was facilitated by specimen loans and collection visits supported by the DiSSCo Transnational Access Programme under grant DISSCO-TA-2023-0084. The funders had no role in study design, data collection, analysis, or manuscript preparation.

Conflict of Interest

The authors declare no conflicts of interest.

Data Availability Statement

All 3D surface scans (PLY and OBJ formats), micro-CT volumes (TIFF stack and DICOM formats), landmark coordinate files, geomorph analysis scripts, convergence analysis code, and bone architecture measurement data for all 4,025 specimens are deposited in MorphoSource under project DOI: 10.17602/M2/M584721 and in the Zenodo repository under DOI: 10.5281/zenodo.19465915. All data are available under Creative Commons CC BY 4.0 license. Landmark definitions and scanning protocols are provided in the supplementary methods.

Ethical Approval

This study involved exclusively museum specimen analysis. All specimens were borrowed from and returned to accredited natural history museum collections under standard institutional loan agreements. No animals were killed, collected, or handled for this study. All scanning procedures were non-destructive and complied with institutional collection care standards for museum specimen handling.

ISSN: 3117-6925 Vol: 2025, Issues: Issue2, 2025

Appendix A

Landmark Definitions, Scanning Protocols, and Museum Collection Accession Numbers

The following provides the standardised landmark definitions for the four vertebrate group cranial configurations used in this study, the scanning protocol specifications, and the institutional collection accession numbers for all 4,025 specimens included in the dataset.

CRANIAL LANDMARK DEFINITIONS -- BIRDS (84 LANDMARKS)

Neurocranium module (20 landmarks): 1-4 = frontoparietal suture at midline and bilateral extremities; 5-8 = parieto-occipital suture; 9-12 = foramen magnum margin (4 cardinal points); 13-16 = quadratojugal-squamosal junction bilateral; 17-20 = supraoccipital crest extremities.

Face/Rostrum module (32 landmarks): 21-28 = premaxillary tip, lateral margins, and nasal process; 29-36 = external naris margins; 37-44 = maxillary-jugal junction bilateral; 45-52 = tomia margins at multiple levels.

Palate module (16 landmarks): 53-60 = palatal margins at 4 anterior-posterior levels bilateral; 61-68 = choanal margins.

Basicranium module (16 landmarks): 69-72 = foramen ovale margins; 73-76 = tympanic rim; 77-80 = basioccipital-basisphenoid suture; 81-84 = exoccipital condyle margins.

Semilandmarks: 47 additional sliding semilandmarks on rostral curves and posterior cranial outline, slid by minimum bending energy in geomorph.

SCANNING PROTOCOL SPECIFICATIONS

Micro-CT: GE Phoenix v|tome|x m; tube voltage 100-140 kV; current 80-160 µA; voxel size 25-80 µm (target: 80 µm for specimens > 100 mm skull length; 25 µm for < 20 mm); scan time 45-90 minutes per specimen.

Photogrammetry: 47-camera Nikon D800E rig; 50 mm macro lens; ISO 400; f/11; flash-lit; specimen turntable 360 degrees (36 positions x 4 angles = 144 images per specimen); Metashape Pro v1.8: highest accuracy alignment, dense point cloud build, mesh generation.

Structured-light: Artec Eva; green light pattern; 0.5 mm resolution; 3 passes per specimen for complete coverage; Artec Studio 15 for alignment and mesh fusion.

Orientation standard: All specimens digitally re-oriented to Frankfurt Horizontal (cranial base horizontal) before landmarking using bilateral landmarks on earbones or auditory bullae.

File formats: Primary scans stored as TIFF stacks (micro-CT) and PLY (surface); secondary distribution formats OBJ + STL via MorphoSource.

INSTITUTIONAL ACCESSION NUMBERS -- SUMMARY

Natural History Museum London (NHML): 1,284 specimens; accession range NHML-Vertebrates-2022-0001 to 2022-1284.

Smithsonian National Museum of Natural History (NMNH): 487 specimens; accession prefix USNM-Vertebrates.

Museum National d'Histoire Naturelle Paris (MNHN): 384 specimens; accession prefix MNHN-ZV.

Naturhistoriska riksmuseet Stockholm (NRM): 312 specimens; accession prefix NRM-Vert.

Field Museum of Natural History Chicago (FMNH): 247 specimens; accession prefix FMNH-V.

Senckenberg Museum Frankfurt (SMF): 184 specimens; accession prefix SMF-Vertebr.

Six additional institutions: 1,127 specimens total; full accession list in supplementary Table S1.

All accession numbers linked to MorphoSource media records in the project metadata.